AD-A182 231 SEPARATION AND REATTACHMENT NEAR THE LEADING EDGE OF A THIN OSCILLATING AIRFOIL(U) MCDONNELL DOUGLAS CORP LONG BEACH CA T CEBECI ET AL DEC 86 MDC-J4847 1/1

UNCLASSIFIED AFOSR-TR-87-0618 F49620-85-C-0063 F/G 20/4 NL

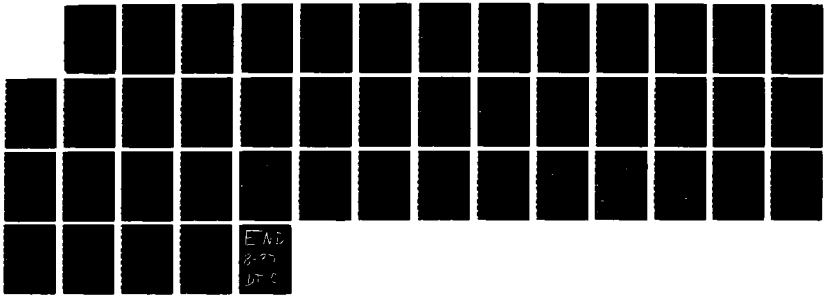

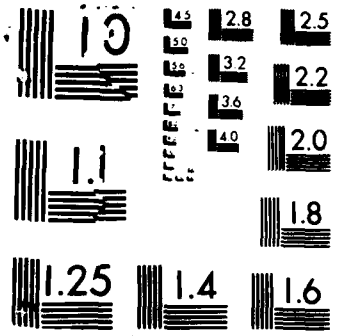
1.0
1.1
1.25
1.4
1.6
1.8
2.0
2.2
2.5
2.8
3.2
3.6
4.0
4.5
5.0
5.6

Report No. MDC J4847

AFOSR-TR-87-0618

SEPARATION AND REATTACHMENT NEAR THE LEADING EDGE OF A THIN OSCILLATING AIRFOIL

by

Tuncer Cebeci, A. A. Khattab and S. M. Schimke
Aerodynamics Research and Technology

December 1986

Work Completed Under
Air Force Office of Scientific Research Contract
F49620-85-C-0063

DOUGLAS AIRCRAFT COMPANY

MCDONNELL DOUGLAS

UNCLASSIFIED

SECURITY CLASSIFICATION OF THIS PAGE

REPORT DOCUMENTATION PAGE

1a. REPORT SECURITY CLASSIFICATION: UNCLASSIFIED	1b. RESTRICTIVE MARKINGS
2a. SECURITY CLASSIFICATION AUTHORITY	3. DISTRIBUTION/AVAILABILITY OF REPORT: Approved for Public Release Distribution Unlimited
2b. DECLASSIFICATION/DOWNGRADING SCHEDULE	
4. PERFORMING ORGANIZATION REPORT NUMBER(S): MDC J4847	5. MONITORING ORGANIZATION REPORT NUMBER(S): AFOSR-TR- 87-0618
6a. NAME OF PERFORMING ORGANIZATION: McDonnell Douglas Corporation, Douglas Aircraft Company; 6b. OFFICE SYMBOL (If applicable)	7a. NAME OF MONITORING ORGANIZATION: AFOSR/ Bolling AFB, DC
6c. ADDRESS (City, State and ZIP Code): 3855 Lakewood Blvd., Long Beach, CA 90846	7b. ADDRESS (City, State and ZIP Code): AFOSR/ BLDG 410, Bolling AFB, DC
8a. NAME OF FUNDING/SPONSORING ORGANIZATION: Air Force Office of Scientific Research; 8b. OFFICE SYMBOL (If applicable): AFOSR/NA	9. PROCUREMENT INSTRUMENT IDENTIFICATION NUMBER: F49620-85-C-0063
8c. ADDRESS (City, State and ZIP Code): Bolling AFB, DC 20332-6448 BLDG 410	10. SOURCE OF FUNDING NOS.

PROGRAM ELEMENT NO.	PROJECT NO.	TASK NO.	WORK UNIT NO.
61102F	2307	A1	

11. TITLE (Include Security Classification): SEPARATION AND REATTACHMENT NEAR THE LEADING EDGE OF A THIN OSCILLATING AIRFOIL

12. PERSONAL AUTHOR(S): TUNCER CEBECI A.A. KHATTAB S.M. SCHIMKE

13a. TYPE OF REPORT	13b. TIME COVERED	14. DATE OF REPORT (Yr., Mo., Day)	15. PAGE COUNT
~~Technical~~ Final	FROM 3/15/85 TO 10/14/86	1986, DECEMBER	38

16. SUPPLEMENTARY NOTATION

17. COSATI CODES			18. SUBJECT TERMS (Continue on reverse if necessary and identify by block number)
FIELD	GROUP	SUB. GR.	Unsteady Flows; Separation, Reattachment; Oscillating Airfoil; Interactive Boundary-Layer Theory; Singularity

19. ABSTRACT (Continue on reverse if necessary and identify by block number)

The evolution of unsteady boundary layers in the vicinity of the leading edge of a thin oscillating airfoil has been examined with a novel numerical method which is able to deal with the movement of the stagnation point and with regions of reverse and separated flow. Solutions to the unsteady boundary-layer equations, with a prescribed pressure distribution which causes flow reversal and separation, demonstrate the importance of numerical steps in distance and time and that a requirement similar to the stability criterion of Courant, Friedrichs and Lewy must be satisfied to avoid numerical errors. At the lower reduced frequencies of the investigation, solutions could not be obtained with this procedure and it was necessary to introduce interaction between the viscous and inviscid flows. The solutions obtained with the interactive method were increasingly different from those without interaction as the reduced frequency was decreased towards zero and, for some combinations of Reynolds number and frequency, exhibited behavior consistent with the instability of separation bubbles.

20. DISTRIBUTION/AVAILABILITY OF ABSTRACT	21. ABSTRACT SECURITY CLASSIFICATION
UNCLASSIFIED/UNLIMITED ☒ SAME AS RPT. ☐ OTIC USERS ☐	UNCLASSIFIED

22a. NAME OF RESPONSIBLE INDIVIDUAL	22b. TELEPHONE NUMBER (Include Area Code)	22c. OFFICE SYMBOL
Dr. James D. Wilson	202/767-4987	AFOSR/NA

DD FORM 1473, 83 APR EDITION OF 1 JAN 73 IS OBSOLETE.

UNCLASSIFIED

SECURITY CLASSIFICATION OF THIS PAGE

Copy number

Report number MDC J4847

SEPARATION AND REATTACHMENT NEAR THE LEADING EDGE OF A THIN OSCILLATING AIRFOIL

Revision date

Revision letter

Issue date December 1986

Contract number F49620-85-C-0063

Prepared by: Tuncer Cebeci, A. A. Khattab and S. M. Schimke

Approved by:

Tuncer Cebeci
Staff Director
Research & Technology
Aircraft Configuration & Performance

D. H. Siegele
Manager
Aircraft Configuration & Performance

DOUGLAS AIRCRAFT COMPANY
MCDONNELL DOUGLAS CORPORATION

Report No MDC J4847

SEPARATION AND REATTACHMENT NEAR THE LEADING EDGE OF A THIN OSCILLATING AIRFOIL

by

Tuncer Cebeci, A.A. Khattab and S.M. Schimke
Aerodynamics Research and Technology

December 1986

Work Completed Under
Air Force Office of Scientific Research Contract
F49620-85-C-0063

Summary

The evolution of unsteady boundary layers in the vicinity of the leading edge of a thin oscillating airfoil has been examined with a novel numerical method which is able to deal with the movement of the stagnation point and with regions of reverse and separated flow. Solutions to the unsteady boundary-layer equations, with a prescribed pressure distribution which causes flow reversal and separation, demonstrate the importance of numerical steps in distance and time and that a requirement similar to the stability criterion of Courant, Friedrichs and Lewy must be satisfied to avoid numerical errors. At the lower reduced frequencies of the investigation, solutions could not be obtained with this procedure and it was necessary to introduce interaction between the viscous and inviscid flows. The solutions obtained with the interactive method were increasingly different from those without interaction as the reduced frequency was decreased towards zero and, for some combinations of Reynolds number and frequency, exhibited behavior consistent with the instability of separation bubbles.

TABLE OF CONTENTS

1.0 INTRODUCTION

The lift and drag characteristics of airfoils at moderate Reynolds numbers can be affected by separation bubbles which occur close to the leading edge and, at high angles of attack, can increase in size to cause stall. The added complexity of unsteady motion such as that associated with the rotor blades of helicopters implies that the flow characteristics are influenced by amplitude and frequency and that, in particular, the stall characteristics can be considerably modified. The investigations of Carr, McAlister and McCroskey (1977), Francis, Keese and Retelle (1983), Daley and Jumper (1984) and Lorber and Covert (1986) examined these effects over limited ranges of the parameters and that of Carr et al. (1977) provides detailed information of the mechanism of dynamic stall of an oscillating airfoil. It appears that stall is associated with flow reversals in the unsteady boundary layer and that these may translate downstream or upstream depending upon various parameters including the radius of the leading edge of the airfoil. At some stage in the cycle, stall occurs and is preceded by a vortex which forms close to the surface and is probably associated with a breakdown of the unsteady boundary layer.

The above physical problems involve laminar, transitional and turbulent flow and their representation requires a numerical calculation procedure which can provide accurate solutions to conservation equations in all regions of flow as well appropriate transition and turbulence models. Here we are concerned with the numerical solution procedure, its development to represent the regions of reverse flow and use to examine the nature of solutions for parameters close to those associated with stall. The emphasis is on regions of flow close to the leading edge of a thin oscillating airfoil and calculations are performed with prescribed pressure gradient and with interaction between solutions of the viscous and inviscid equations. With the configuration chosen, an analytical solution for the potential flow equations was available.

Previous consideration of steady boundary layers and their solution by an interactive procedure, has been reported by Cebeci, Stewartson and Williams (1981) for a model problem consisting of a thin ellipse at incidence. Their study showed that the solutions were well behaved and unseparated provided the angle of attack was less than 1.155 degrees. At higher angles, separation occurred with an associated singularity which was overcome by the use of the

interactive procedure and results were obtained for small regions of separated flow. There is, however, a limiting size of separation bubble beyond which Cebeci, et al. (1981) could not obtain solutions and this may be related to the physical phenomenon of open separation and stall. A similar result was obtained by Stewartson, Smith and Kaups (1982) who used a triple-deck approach and found that their calculations of separation bubbles could break down with a small increment in pressure gradient. They also observed that their solutions were not unique and their results may imply that large separation bubbles cannot exist in laminar flows at high Reynolds numbers.

The unsteady-flow calculations reported here were obtained with Keller's box method (1974) for the solution of the boundary-layer equations. In regions of flow reversal, a requirement similar to the stability criterion of Courant, Friedrichs and Lewy (CFL), see Isaacson and Keller (1966), is satisfied by the use of the characteristic box procedure discussed by Keller (1978) and Cebeci (1986) and the interactive procedure is based on the Hilbert-integral previously used by Cebeci et al. (1981). This combination of methods represents the best possible approach available to the authors and allows the importance of the stability criterion to be examined as well as the structure of the solutions. Of necessity, a limited number of parameters is considered but encompasses a range of relevance to oscillating airfoils.

The flow configuration under consideration, equations, initial and boundary conditions are examined in the following section which is followed by a brief description of the solution procedure. The results are presented and discussed in Section 4 and the paper ends with a summary of the more important conclusions.

2.0 FLOW CONFIGURATION, CONSERVATION EQUATIONS, INITIAL AND BOUNDARY CONDITIONS

We consider flow over an ellipse with a thickness ratio $\tau(\equiv b/a)$ much less than unity at an angle of attack α. The body surface is defined by

$$x = -a\cos\theta, \quad y = a\tau\sin\theta \qquad -\pi \le \theta \le \pi$$

and the corresponding external velocity for steady flow can be deduced from inviscid flow theory to be

$$\overline{u_e^o}(s,t) = \frac{\xi + \xi_o}{\sqrt{1 + \xi^2}} \tag{1}$$

Here $\overline{u_e^o}(s,t)$ denotes a dimensionless velocity, $u_e^o/u_\infty(1 + \tau)$, the parameter ξ denotes a dimensionless distance from the nose related to the x- and y-coordinates of the ellipse by $x = 1/2\ a\tau^2\xi$, $y = a\tau^2\xi$, and ξ_o $(\equiv\alpha/\tau)$ represents a dimensionless angle of attack. The parameter ξ is related to the surface distance s by

$$s = a\tau^2 \int_0^\xi (1 + \xi^2)^{1/2} d\xi$$

The boundary-layer equations for unsteady incompressible laminar flows on oscillating airfoils are well known and can be written as

$$\frac{\partial u}{\partial s} + \frac{\partial v}{\partial n} = 0 \tag{2}$$

$$\frac{\partial u}{\partial t} + u\frac{\partial u}{\partial s} + v\frac{\partial u}{\partial n} = \frac{\partial u_e}{\partial t} + u_e\frac{\partial u_e}{\partial s} + \nu\frac{\partial^2 u}{\partial n^2} \tag{3}$$

Solutions to these equations are usually obtained for prescribed boundary conditions given by

$$n = 0, \quad u = v = 0; \quad n = n_e, \quad u = u_e(s,t) \tag{4}$$

and we shall refer to this as the standard problem. In the interactive problem we determine $u_e(s,t)$ partly from inviscid theory and partly from the pressure

distribution resulting from the blowing velocity d/ds ($u_e\delta^*$) induced by the boundary layer. Thus we write

$$u_e(s,t) = u_e^o(s,t) + u_c(s,t) \tag{5}$$

where $u_e^o(s,t)$ is the inviscid velocity and $u_c(s,t)$ is related to the blowing velocity by a variation of the Hilbert integral

$$u_c(s,t) = \frac{1}{\pi} \int_{-\infty}^{\infty} \frac{d}{ds}(u_e\delta^*) \frac{d\sigma}{s-\sigma} \tag{6}$$

which is valid for straight walls but can be generalized to airfoils as discussed by Cebeci and Clark (1984). The freestream velocity, consistent with Eq. (1) has the form

$$\overline{u_e^o}(s,t) = \frac{\xi + \xi_o(1 + A\sin\omega t)}{\sqrt{1+\xi^2}} \tag{7}$$

where A is an amplitude parameter and ω is a dimensional frequency.

For attached flows, the effect of $u_c(s,t)$ is generally weak but is enhanced in the neighborhood of separation as can be surmised by noting that the integrand in Eq. (6) would otherwise develop a strong singularity at separation and cause the solutions to break down further downstream. As discussed by Cebeci, et al. (1981), it is sufficient to replace Eq. (6) by

$$u_c(s,t) = \frac{1}{\pi} \int_{s_a}^{s_b} \frac{(u_e\delta^*)'}{s-\sigma} d\sigma \tag{8}$$

where the prime denotes differentiation with respect to s and s_a and s_b denote the beginning and the end of the interaction region.

To complete the formulation of the problem, upstream boundary conditions must be specified in the (t,n) plane at some $s = s_o$ as well as initial conditions in the plane (s,n) at t = 0. If steady-flow conditions prevail at t = 0, the initial conditions can be obtained easily for both surfaces by solving the conservation equations for steady flow which, in this case, are given by Eq. (2) and by

$$u \frac{\partial u}{\partial s} + v \frac{\partial u}{\partial n} = u_e \frac{du_e}{ds} + \nu \frac{\partial^2 u}{\partial n^2} \tag{9}$$

There is no problem with the initial conditions for Eqs. (2) and (9) since the calculations start at the stagnation point where they admit similarity solutions.

The generation of the upstream boundary conditions for Eqs. (5) and (6) requires a special numerical procedure. Since the complete velocity profile distribution on a previous time line is known, solutions can be determined on the next time line by an explicit method. If we wish to avoid stability problems, however, an implicit method is required and generation of a starting profile on the new time line becomes a problem.

In order to explain the problem further, it is instructive to see what happens to the stagnation point as a function of time. For this purpose let us consider Eq. (7). Since $\bar{u}_e^o = 0$ at the stagnation point, its location, ξ_s, based on the external streamlines is given by

$$\xi_s = -\xi_o(1 + A \sin\omega t) \tag{10}$$

Figure 1 shows the variation of the stagnation point with time for one cycle according to Eq. (10) with $A = 1$, $\omega = \pi/4$. We see that when $t = 2$, the stagnation point ξ_s is at $-2\xi_o$, and when $t = 6$, it is at 0, etc. If ξ_s were fixed, we could assume that $u = 0$ at $\xi = -\xi_o$ for all time and all n, but this is not the case. It is also possible to assume that the stagnation point is coincident with zero u-velocity for a prescribed time but we should note that the stagnation point defined by Eq. (10) is based on the vanishing of the external velocity. For a time-dependent flow, this does not imply that the u-velocity must be zero across the layer at a given ξ-location and specified time; indeed flow reversals can occur due to the movement of the locus of zero u-velocity across the layer and can cause numerical instabilities which require the use of special numerical schemes as discussed by Cebeci and Carr (1981).

3.0 SOLUTION PROCEDURE

With the upstream boundary conditions determined by the procedure of Cebeci and Carr (1981) and with the initial conditions obtained from the solution of Eqs. (2) and (9) subject to the boundary conditions given by Eqs. (4) to (6), Eqs. (2) and (3) can be solved for both standard or inverse problems. In practice a standard procedure is used up to a specified ξ-location after which the calculations may proceed by either standard or inverse procedures. For example, the evolution of the boundary layer on an oscillating airfoil with prescribed pressure distribution is determined with the standard procedure and the inverse procedure is used after a short distance from the leading-edge region where the inviscid and viscous flow equations are solved interactively.

To solve the equations for both standard and inverse problems we use modified forms of Keller's box scheme. The Mechul function formulation of Cebeci (1976) is used in the inverse case and treats the external velocity as an unknown. Before we describe this formulation and the solution procedure, it is convenient to write Eqs. (2) to (4) in a form more suitable for computation. To achieve this we define dimensionless distances η and $\bar{s}$ and time τ by,

$$\eta = \left[\frac{R(1 + t_1)}{2t_1^2}\right]^{1/2} \frac{n}{a}, \qquad \bar{s} = \frac{s}{at_1^2}, \qquad \tau = \frac{u_\infty(1 + t_1)}{at_1^2}\, t \tag{11a}$$

with $R = 2au_\infty/\nu$, and a dimensionless stream function f by

$$\psi(s,n,t) = [(1 + t_1)au_\infty \nu t_1^2]^{1/2} f(\bar{s},\eta,\tau) \tag{11b}$$

These relations may be introduced into Eqs. (2) and (3) to give, with primes denote differentiation with respect to η,

$$f''' + \frac{\partial w}{\partial \tau} + w \frac{\partial w}{\partial \bar{s}} = \frac{\partial f'}{\partial \tau} + f' \frac{\partial f'}{\partial \bar{s}} - f'' \frac{\partial f}{\partial \bar{s}} \tag{12}$$

where

$$w = \frac{u_e}{u_\infty(1 + t_1)}, \qquad f' = \frac{u}{u_\infty(1 + t_1)}$$

The boundary conditions follow from Eqs. (4) to (6) and can be written as

$$\eta = 0, \qquad f = f' = 0, \tag{13}$$

$$\eta = \eta_e, \qquad f' = w, \qquad w = \bar{u}_e^o + \varepsilon \int_{\bar{s}_a}^{\bar{s}_b} \frac{d\Delta}{d\bar{s}} \frac{d\bar{\sigma}}{\bar{s} - \bar{\sigma}}$$

Here Δ denotes a dimensionless displacement thickness given by

$$\Delta(\bar{s},\tau) = \eta_e w - f_e \tag{14}$$

and ε is a parameter defined by

$$\varepsilon = \frac{1}{\pi t_1} \left[\frac{2}{R(1 + t_1)}\right]^{1/2} \tag{15}$$

To pave the way for the description of the numerical method, we define a new variable

$$\theta = \frac{\partial f}{\partial \bar{s}} \tag{16}$$

and write Eq. (12) as

$$f''' + f''\theta + \frac{\partial w}{\partial \tau} + w \frac{\partial w}{\partial s} = \frac{\partial f'}{\partial \tau} + f' \frac{\partial f'}{\partial s} \tag{17}$$

where the overbar has been omitted. We use Keller's box method (1974) to solve this equation. In regions of no flow reversal the so-called standard box method is used and where there is flow reversal, this is replaced by the characteristic scheme which is based on the solution of Eq. (17) along streamlines as described by Keller (1978) and Cebeci (1986). This scheme allows the step sizes in the τ and s-directions to be automatically adjusted to ensure that the region of backflow determined by the local streamlines does not violate a condition like the Courant, Friedrichs and Lewy (CFL) stability criterion. Although the zig-zag scheme of Krause et al. (1968) can also be used for this purpose, it can be inaccurate in regions of large flow reversal since the orientation of numerical mesh is chosen a priori, as discussed by Cebeci (1986) and later in this paper.

To solve Eqs. (17) and (14) with the box scheme and the Mechul function formulation, we let

$$f' = e \tag{18}$$

and introduce a new function g defined by

$$e' = g \tag{19a}$$

and with w(x) treated as unknown

$$w' = 0 \tag{19b}$$

and write Eqs. (16) and (17) and their boundary conditions as

$$\theta' = \frac{\partial e}{\partial s} \tag{19c}$$

$$g' + g\theta + \frac{\partial w}{\partial t} + w\,\frac{\partial w}{\partial s} = \frac{\partial e}{\partial \tau} + e\,\frac{\partial e}{\partial s} \tag{19d}$$

$$\eta = 0, \qquad f = e = 0;$$

$$\eta = \eta_e, \qquad e = w, \qquad w = \overline{u_e^o} + \varepsilon \int_{s_a}^{s_b} \frac{d\Delta}{ds}\,\frac{d\sigma}{s-\sigma} \tag{20}$$

To write the difference equations for the system given by Eqs. (19) and (20), we consider a net cube in which the net points are denoted by

$$\begin{aligned} s_o &= 0, & s_i &= s_{i-1} + r_i & i &= 1, 2, \ldots, I \\ \tau_o &= 0, & \tau_n &= \tau_{n-1} + k_n & n &= 1, 2, \ldots, N \\ \eta_o &= 0, & \eta_j &= \eta_{j-1} + h_j & j &= 1, 2, \ldots, J \end{aligned} \tag{21}$$

where $r_i = \Delta s_i$, $k_n = \Delta \tau_n$ and $h_j = \Delta \eta_j$.

The difference approximations to represent Eqs. (19a) and (19b) are obtained by averaging about the midpoint $(s_i, \tau_n, \eta_{j-1/2})$,

$$h_j^{-1}(e_j^{i,n} - e_{j-1}^{i,n}) = g_{j-1/2}^{i,n} \tag{22a}$$

$$h_j^{-1}(w_j^{i,n} - w_{j-1}^{i,n}) = 0 \tag{22b}$$

where, for example,

$$e_{j-1/2}^{i,n} = \frac{1}{2}\,(e_j^{i,n} + e_{j-1}^{i,n}) \tag{23}$$

The finite difference approximations to Eqs. (19c) and (19d) are obtained by centering all quantities except θ at the center of the cube ($s_{i-1/2}$, $\tau_{n-1/2}$, $n_{j-1/2}$) by taking the values of each say q, at the four corners of the box, that is,

$$q_{j-1/2}^{i-1/2,n} = \frac{1}{2}\,(q_{j-1/2}^{i,n} + q_{j-1/2}^{i-1,n}) = \frac{1}{4}\,(q_j^{i,n} + q_{j-1}^{i,n} + q_{j-1}^{i-1,n}) \tag{24a}$$

The centering of θ is done by writing it as

$$\theta_{j-1/2}^{i-1/2,n-1/2} = \frac{1}{2}\,(\theta_j^{i-1/2,n} + \theta_{j-1}^{i-1/2,n-1/2}) \tag{24b}$$

In this notation, the difference approximations to Eqs. (19c) and (19d) can be written in the form:

$$h_j^{-1}(\theta_j - \theta_{j-1}) = r_i^{-1}(\bar{e}_i - \bar{e}_{i-1}) \tag{25a}$$

$$h_j^{-1}(\bar{g}_j - \bar{g}_{j-1}) + \bar{g}_{j-1/2}\theta_{j-1/2} + k_n^{-1}(\bar{w}_n - \bar{w}_{n-1}) + r_i^{-1}[\bar{w}_{j-1/2}(\bar{w}_i - \bar{w}_{i-1})]$$

$$= k_n^{-1}(\bar{e}_n - \bar{e}_{n-1}) + r_i^{-1}[\bar{e}_{j-1/2}(\bar{e}_i - \bar{e}_{i-1}) - \bar{g}_{j-1/2}(\bar{f}_i - \bar{f}_{i-1})] \tag{25b}$$

where, for example,

$$\bar{e}_j = e_j^{i-1/2,n-1/2}, \quad \bar{e}_n = e_{j-1/2}^{i-1/2,n}, \quad \bar{e}_i = e_{j-1/2}^{i,n-1/2}, \quad \theta_j = \theta_j^{i-1/2,n-1/2} \tag{26}$$

Following the procedure of Cebeci, et al. (1981) the boundary condition involving the Hilbert integral in Eq. (20) can be written in the form

$$w_J^{i,n} - c_{ii}\,\varepsilon(\eta_J\, w_J^{i,n} - f_J^{i,n}) = T_J^{i,n} \tag{27}$$

where c_{ii} is the matrix of interaction coefficients defining the relationship between the dimensionless displacement thickness and external flow and the parameter $T_J^{i,n}$ represents terms where values are assumed to be known. It is given by

$$T_J^{i,n} = (\overline{u_e^o})^{i,n} + \varepsilon \sum_{m=1}^{i-1} c_{im}\,\Delta_J^{m,n} + \varepsilon \sum_{m=i+1}^{\ell} c_{im}\Delta_J^{m,n} \tag{28}$$

To compute the additional unknown of Eq. (27), we write Eq. (18) in the form

$$h_j^{-1}(f_j^{i,n} - f_{j-1}^{i,n}) = e_{j-1/2}^{i,n} \tag{29}$$

so that the system consisting of Eqs. (22), (25), and (29) can be solved subject to the boundary conditions given by Eq. (27) and which follow from Eq. (20),

$$f_o = \theta_o = e_o = 0; \qquad e_J = w_J \tag{30}$$

The above system can be linearized by Newton's method and the resulting linear system solved by the block elimination procedure described in Cebeci and Bradshaw (1984) for both standard and inverse formulations. In the former case, it is sufficient to set $\varepsilon = 0$ in Eq. (27) so that w is equal to $\bar{u}_e^o$.

We follow the above solution procedure when there is no flow reversal across the layer. If separation is identified from the values of $u_j^{i,n}$, we use the characteristic scheme which has recently been described by Cebeci (1986) in relation to the standard problem of computing the impulsively started laminar flow over a circular cylinder. The solution procedure in this case is similar with small adjustments due to the manner in which the difference equations are adjusted to the modified form of Eq. (19d). Noting the definition of local streamlines, we write

$$d\tau = \frac{ds}{e} \tag{31}$$

If we denote distance in this direction by q and the angle that it makes with the τ-axis by α, then Eq. (19d) can be written as

$$g' + g\theta + \beta = \lambda \frac{\partial e}{\partial q} \tag{32}$$

where

$$\lambda = \sqrt{1 + e^2} \tag{33a}$$

$$\alpha = \tan^{-1} e \tag{33b}$$

$$\beta = \frac{\partial w}{\partial \tau} + w \frac{\partial w}{\partial s} \tag{33c}$$

The finite-difference approximations to Eq. (32) are written along the streamline direction (see Fig. 2) at

$$\frac{h_j^{-1}}{2}\left(q_j^{i,n} - q_{j-1}^{i,n}\right) + \frac{h_j^{-1}}{2}\left(q_j^{m,n-1} - q_{j-1}^{m,n-1}\right) + \beta^P$$

$$+ \frac{1}{2}\left(q_{j-1/2}^{i,n} + q_{j-1/2}^{m,n-1}\right)\theta_{j-1/2}^P = \frac{1}{2}\left(\lambda_{j-1/2}^{i,n} + \lambda_{j-1/2}^{m,n-1}\right)\frac{e_{j-1/2}^{i,n} - e_{j-1/2}^{m,n-1}}{\Delta q_{j-1/2}} \tag{34}$$

where

$$\Delta q_{j-1/2} = k_n/\cos\alpha_{j-1/2} \tag{35}$$

The relation between $\theta_{j-1/2}^P$ and those values of θ centered at $(i-1/2,n-1/2)$ and $(i-3/2,n-1/2)$ are

$$\theta_{j-1/2}^P = \frac{\theta_{j-1/2}^{i-3/2} - \theta_{j-1/2}^{i-1/2}}{s_{i-3/2} - s_{i-1/2}}\left(s^P - s_{i-3/2}\right) + \theta_{j-1/2}^{i-3/2} \tag{36}$$

The solution of Eq. (12) subject to the boundary conditions given by Eq. (13) is achieved by solving the system of equations given by Eqs. (18), (19) and (20) (standard scheme) when there is no flow reversal. When calculated results reveal flow reversal ($e_j < 0$), further iterations at that location make use of the characteristic scheme which seeks the solution of Eqs. (18), (19a,b,c) and (32) for $e_j < 0$ and the regular scheme for $e_j > 0$. This switch from one scheme to another continues to allow quadratic convergence and ensures that numerical instabilities are avoided provided that the step lengths in the τ- and s-directions are "properly" selected as we shall discuss in the following section.

4.0 THE QUESTION OF SINGULARITY ON AN OSCILLATING AIRFOIL

The problem of a circular cylinder impulsively started from rest has served as a model problem with which to examine unsteady boundary layers and the nature of their solutions in the presence of large flow reversal. Noteworthy contributions have been made by Cebeci (1979), van Dommelen and Shen (1982), Cowley (1983) and Ingham (1984), and show that at large times the distribution of displacement thickness has a steep rise near the location of zero wall shear and with consequent tendency for calculations to break down. The suggested values for the time and location of zero wall shear and peaking of the displacement velocity, $[d/ds(u_e \delta^*)]$ vary slightly, probably due to differences in the calculation methods. The explanation for the breakdown of the calculations has been provided by Cebeci (1986) who demonstrated that numerical calculations must satisfy a CFL-like stability criterion. If this is done, it is expected that the location of the singularity associated with unsteady flow and large time will correspond exactly to that of steady flow, namely $\theta = 105°$, rather than $\theta = 111°$. The same situation cannot be expected with oscillating airfoils where the solutions are cyclic and do not tend to a steady state.

The present study examines the nature of solutions to the boundary-layer equations for the flow on an oscillating airfoil, which can give rise to extensive regions of flow reversal and separation. Here flow reversal implies the existence of negative wall shear and separation is taken to correspond to situations where calculations with a prescribed pressure distribution breakdown due to a singularity. The calculations were made for three values of ω with $\xi_o = 1$ and $A = -1/2$. With the choice of $\omega = 0.001$, 0.01 and 0.10, the maximum value of ξ_{eff}, defined by

$$\xi_{eff} = \xi_o(1 + A \sin\omega t)$$

is sufficient to provoke separation with a strong singularity. For example, the maximum value of ξ_{eff} is 1.5 at $\omega t = 270$ and the flow conditions closely resemble a steady separated flow at the smaller frequencies $\omega = 0.001$ and 0.01. Since the value of ξ_{eff} corresponding to steady flow separation is 1.115, we would expect the calculations to break down before $\omega t = 270°$ due to the singularity. For the higher frequency case ($\omega = 0.10$), we expect the solutions to break down later than $\omega t = 270°$ with flow reversals occurring in the range $270° < \omega t < 360°$.

The calculations were arranged to parallel those previously performed for a circular cylinder and reported by Cebeci (1986). Thus both the zig-zag and the characteristic box schemes were used first with time and distance steps which were chosen arbitrarily and subsequently with values in agreement with the stability criterion. The results of Fig. 3 for $\omega = 0.10$ were obtained with the zig-zag box scheme by Cebeci, Khattab and Schimke (1984) for a $\Delta\xi$ spacing specified such that $\Delta\xi_1 = 0.01$ up to $\xi = 1.7$, $\Delta\xi_1 = 0.005$ for $1.7 < \xi < 4$ and $\Delta\xi_1 = 0.01$ for $4 < \xi < 8$; the time steps k_n were 10 degrees degrees for $0 < \omega t < 260$, 5 degrees for $260 < \omega t < 295$, and 1.25 degrees for $295 < \omega t < 360$. The calculations broke down at $\omega t = 310°$, indicating flow separation at this location.

Fig. 3a shows that the variation of the displacement thickness

$$\tilde{\delta}^* = \frac{\delta^*}{a}\left(\frac{1+\tau}{\tau}\right)\frac{1}{c\pi} \tag{25}$$

is generally smooth except in the neighborhood of $\xi = 2.12$ and for $\omega t = 308.75°$. The first sign of irregularity is the steepening of the slope of $\tilde{\delta}^*$ when $\omega t = 300°$ and a local maximum of $\tilde{\delta}^*$ occurs at $\xi = 2.12$ when $\omega t = 308.75°$. When the same results are plotted for a displacement velocity, $(d/d\xi)(u_e\tilde{\delta}^*)$, (Fig. 3b), we observe that the steepening of the displacement velocity as the peak moves form $\xi = 2.125$ to 2.08 with ωt changing from 300 to 308.75 degrees. It should be noted that the maximum value of displacement velocity moves towards the separation point with increasing ωt and the same behavior will be shown to occur for the circular cylinder discussed below. As shown in Fig. 3c, the wall shear parameter f_w'' shows no signs of irregularity for $\omega t \leq 308.75°$ but a deep minimum in f_w'' occurs near $\xi = 2.15$, i.e. near the peak of $\tilde{\delta}^*$.

It is interesting and useful to compare the results presented in Fig. 3 for an oscillating airfoil with those obtained by Cebeci (1982) for a circular cylinder started impulsively from rest, Fig. 4, and obtained with the same zig-zag scheme. As in the case of the oscillating airfoil, the flow separates and remains smooth up to the separation point. However, just downstream of separation with increasing time, a singularity seems to develop in the neighborhood of $\theta = 112°$ and $t \approx 3.0$ and it was not possible to continue the boundary-layer calculations beyond this time and angular location. From Fig. 4a we see that the variation of displacement thickness is smooth for values of θ less

than 108° and it begins to steepen thereafter. The same results are plotted in Fig. 4b to demonstrate that the displacement velocity exhibits a maximum which increases rapidly with time, as in Fig. 3b, with the maximum shifting towards the location of separation with increasing time. The results of local skin-friction coefficients, Fig. 4c, follow similar trends to those obtained for the oscillating airfoil with the distributions passing through zero with no signs of irregularity and no breakdown before the time corresponding to the singularity.

The calculations which led to Fig. 3 were repeated with the characteristic box scheme using the same coarse variations of k_n and $\Delta\xi_i$ and the results were identical to those obtained with the zig-zag scheme up to $\omega t = 280$. At $\omega t = 282.5$, the solutions of the zig-zag scheme were smooth and free of wiggles but those of the characteristic box scheme exhibited oscillations in $f_w^{\bullet}$ which led to their breakdown. The solutions with the zig-zag scheme, however, continued without numerical difficulties until $\omega t = 310$, where oscillations appeared and led to the breakdown of the solutions at the next time step.

The characteristic box was used subsequently with values of $\Delta\xi_i$ fixed as before and with values of k_n determined in accord with the stability requirement as shown in Table 1. This procedure avoided the breakdown of the solutions and, as can be seen from Fig. 5, the maximum value of β increases considerably with ωt so that the solutions required correspondingly smaller values of the time step. It is interesting to note that the wall-shear distributions of Fig. 6 are uninfluenced by the mesh at $\omega t = 280$ and 310 but, for $\omega t > 310$, the coarse mesh leads to large values of β and breakdown of the solutions.

Figure 7a shows the distributions of displacement thickness for values of ωt from 260° up to 360° and completes the cycle. The results up to 300° were identical with those of Fig. 3a with rapid increase of the displacement thickness corresponding to the increasing extent of flow reversal, as shown by the wall-shear distributions of Fig. 7b. It can also be seen from this figure that the maximum displacement thickness and minimum wall shear move upstream with increasing ωt for values of ωt up to 324.5°; this feature was also observed in the calculations performed for the circular cylinder and shown in Fig. 4.

Table 1. The distribution of step sizes in ωt for $\omega t = 0.1$ in accordance with the requirements of the stability parameter β

ωt	k_n
0 - 240	10°
240 - 255	5°
255 - 261	3°
261 - 265	2°
265 - 284	1°
284 - 305	0.5°
305 - 320	0.25°
320 - 360	0.5°

The results obtained with the zig-zag scheme and values of k_n determined by the characteristic scheme for the oscillating airfoil were identical to those discussed above, and similar correspondence was obtained with the calculations performed for the circular cylinder.

Figures 8 and 9 show the distributions of wall shear and displacement thickness for two smaller frequencies $\omega = 0.01$ and 0.001. As expected, the critical value of the reduced angle which corresponds to separation, is smaller than that for the higher frequency and closer to that of the steady state, $\xi = 1.16$. For $\omega = 0.01$, the breakdown of the solutions occurs at $\omega t = 226°$, which corresponds to an effective reduced angle of $\xi_{eff} = 1.360$; for $\omega = 0.001$, the corresponding values are $\omega t = 204°$ and 1.203. We also note from Figures 8a and 8b that the flow is a "little" unsteady even at these frequencies, and the solutions do not break down with the appearance of flow reversal, which increases in extent as ω changes from 0.001 and 0.01.

5.0 INTERACTION AS AN ANSWER TO THE QUESTION OF SINGULARITY

The interaction procedure discussed in Section 3 has been applied to the flow problem examined previously in Section 4 with the standard method and the results are shown in Figures 10 to 14 and discussed below. In contrast to the standard problem, which makes the implicit assumption of infinite Reynolds number, the interaction requires specification of a finite Reynolds number. A thickness ratio τ has also to be specified and, since the definition of ε involves R and τ, the calculations are performed for specified values of ε. In all cases shown, the calculations made use of time steps determined by the characteristic scheme in agreement with the stability requirement. This was not done in the calculations of Cebeci et al. (1984) and the solutions exhibited oscillations which stemmed from the numerical method.

The present calculations were performed in the following way. For all values of time with ωt ranging from 0 to 360°, the standard method and the leading-edge region procedure of Cebeci and Carr (1981) were used to generate initial conditions at a short distance from the leading edge, $\xi = 0.5$. With these initial conditions and for each value of ωt, the inverse method was used to calculate the unsteady flow from $\xi = 0.5$ to 10, for the specified value of ε. Since the system of equations is now elliptic, sweeps in the ξ-direction were necessary to achieve a converged solution; around three sweeps were required where flow reversal was encountered and a single sweep sufficed where it did not. It is to be expected that the value of ε will influence the number of sweeps and, since it is linked to physical parameters, will affect the singularity and the size of the bubble.

Figures 10 and 11 show the results for $\omega = 0.001$ and 0.01 with $\varepsilon = 10^4$. They are nearly the same as those obtained by the standard method and shown in Figures 8 and 9 prior to flow reversal where the influence of the Reynolds number is small and increase after flow reversal. In the case of $\omega = 0.001$, for example, the standard method predicts flow reversal around $\xi_{eff} = 1.19$ (see Fig. 9) and with interaction (Fig. 10) this effective angle is between 1.219 and 1.254. The maximum negative value of the wall-shear parameter f_w'' obtained with the standard method is around -0.03 at $\xi_{eff} = 1.199$ and may be compared with the maximum value of f_w'' of -0.14 at $\xi_{eff} = 1.286$ obtained with interaction. As expected, the interaction allows the calculations to be performed

at higher angles of attack than those achieved with the standard method. For $\omega = 0.001$, the maximum α_{eff} for which calculations can be performed with the standard method is 1.199 with breakdown occurring at $\xi_{eff} = 1.209$; the corresponding values with interaction are 1.286 and 1.287. Comparison of wall-shear results with both procedures and $\omega = 0.001$ indicates that the extent of the recirculation region $\Delta\xi$ is around 0.5 for the standard case, and around 2.5 for the interactive case. The solutions do not have a singularity in the former case but do contain flow reversals and this suggests that time-dependent flows can be calculated without using an inverse procedure. As the angle of attack exceeds $\xi_{eff} = 1.199$ for $\omega = 0.001$, a singularity develops and requires an inverse procedure as in two-dimensional steady flows. This procedure allows the calculation of larger regions of reverse flow where the flow is now separated.

We see a similar picture with the greater unsteadiness corresponding to $\omega = 0.01$, for which the standard method allows calculations up to an effective angle of attack of 1.354 (Fig. 8a), a value considerably higher than 1.199 obtained at $\omega = 0.001$. The first flow reversal occurs shortly after $\xi_{eff} = 1.294$ and breakdown occurs at $\xi_{eff} = 1.360$ with maximum negative wall shear values of -0.14 at $\xi_{eff} = 1.354$ and -0.035 at $\xi_{eff} = 1.315$. The extent of the maximum reverse-flow region is now 1.5, considerably larger than for $\omega = 0.001$, and indicates that the more unsteady nature of the flow produces a bigger region of reverse flow free from singularities. For this value of ω, the interactive scheme increases the value of ξ_{eff} for which solutions can be obtained to 1.424 with breakdown occurring shortly after this value at 1.428 (see Fig. 11). The first flow reversal occurs after $\xi_{eff} = 1.315$ with maximum negative wall shear equal to -0.19 at $\xi_{eff} = 1.424$, and the extent of the recirculation region has now increased by about 30%. Comparison of maximum wall shear values, f_w'', at a similar value of ξ_{eff} indicates that those computed with the interactive scheme are lower than those with the standard scheme so that, for example, the interactive scheme gives $(f_w'')_{max} = -0.04$ at $\xi_{eff} = 1.36$ compared to -0.14 at $\xi_{eff} = 1.354$ with the standard method (Fig. 8a).

Figure 12 shows that the size of the reverse-flow region increases with Reynolds number but the effective angle of attack for which solutions can be obtained is only slightly reduced, changing from 1.428 for $\varepsilon = 10^4$ to

around 1.415 for $\varepsilon = 10^5$. It is interesting to note that the interactive solutions do not have any flow reversal at $\xi_{eff} = 1.315$ with $\varepsilon = 10^4$.

Figures 13 and 14 show the results for $\omega = 0.1$ with values of ε of 10^4 and 10^5 and they are again similar to those obtained by the standard method, as shown in Figure 7, prior to flow reversal where the influence of Reynolds number is small. After flow reversal, the differences between the results obtained with the standard and interactive methods increase as the Reynolds number decreases. It is clear that the solutions are free from the numerical "wiggles" encountered when the stability criterion was not met.

Comparison of results obtained at the two Reynolds numbers for $\omega = 0.1$ indicates that the interaction does not reduce the maximum negative value of the wall shear parameter as it did with lower frequencies. For example, f''_w at $\omega t = 360°$ is around -0.19 with the standard scheme and around -0.30 at $\varepsilon = 10^4$ and around -0.35 at $\varepsilon = 10^5$ with the interactive method. The maximum value of negative wall shear calculated with interaction is considerably greater than its corresponding value obtained with the standard method at the end of one complete cycle. Furthermore, the behavior of the wall shear is not monotonic without interaction so that, for example, f''_w reaches a maximum value equal to -0.25 around $\omega t = 331°$ and then decreases to -0.195 at $\omega t = 360°$. With interaction this is not the case with the maximum negative value of f''_w continuously increasing with ωt.

The results of Figures 7, 13 and 14 for $\omega = 0.1$ are for an unsteady flow and are unlike those for two other values of ω in that they are free from singularities. For this reason, even though the results in the reverse flow region and thereafter are different due to the Reynolds number effect, the extent of the reverse-flow region is essentially the same and is consistent with the results obtained at lower frequencies in the absence of flow separation even though the extent of the reverse-flow region is reduced at the lower Reynolds numbers.

The results obtained with $\omega = 0.001$ can usefully be compared with the steady-state results of Cebeci et al. (1981) shown in Figure 15. We might expect that the small unsteadiness associated with this frequency will lead to results very similar to those of steady state. Inspection of Figures 10 and 15 shows that

although this is correct in general terms, the answers are quantitatively different. As can be seen, the maximum effective angle at which solutions can be obtained is greater in the unsteady case by some 7%. There are differences in the two calculation procedures but it is unlikely that they are responsible for this difference. On the other hand, it is possible that the difference in the negative wall shear values may have been influenced by the use of the FLARE approximation in the steady-state solutions. Nevertheless, the unsteady nature of the flow with $\omega = 0.001$ is clear, in spite of this very low reduced frequency.

6.0 CONCLUDING REMARKS

The following principle conclusions may be drawn from the preceding text.

1. A calculation method has been developed to represent flows around oscillating airfoils. It is based on a similar approach used for steady flows with separation and involves interaction between inviscid and viscous-flow equations. The coupling technique is similar to that described by Veldman (1981) and Cebeci et al. (1981) for steady flows. This interactive method has been used to calculate separation and reattachment near the leading edge of a thin oscillating airfoil and has been shown to give rise to rapid convergence similar to that obtained in steady flows, Cebeci et al. (1986).

2. The accuracy of the results obtained from the solution of the boundary-layer equations has been examined with emphasis on regions of flow reversal and separation where the characteristic box scheme is used. Attempts to improve accuracy by ad hoc changes to the finite-difference mesh failed and revealed the need for a procedure which would automatically guarantee accuracy by the selection of an appropriate mesh. This was achieved through a stability criterion, similar to that of Courant, Friedrichs and Lewy. The combination of this requirement and the characteristic box scheme led to accurate solutions and showed that the mesh requirements were extremely severe in the region of large flow reversals.

3. Calculations have been performed for a range of reduced frequencies from 0 to 0.1. They show that increased unsteadiness allows results to be obtained at higher angles of attack before the solutions break down; indeed in the case of the highest frequency there was no breakdown. The calculations with the standard method led to regions of flow reversal which were limited in their extent by the singularity except at the highest frequency. The interactive procedure removed this singularity and resulted in larger regions of flow reversal which involved separation at higher angles of attack.

   The calculated maximum angles of attack were, however, modest and regions of separated flow were small. This is consistent with the behavior of steady laminar flows which can only sustain small separation bubbles.

The unsteady nature of the flow at the highest frequency allowed the calculation of large regions of flow reversal and it is expected that yet higher frequencies will lead to even larger regions of flow reversal. This in turn will permit calculations to be performed at larger angles of attack where the occurrence of the singularity will require the use of the interactive procedure. The gains in angles of attack are again likely to be limited by the ability of the laminar flow to sustain separation bubbles.

4. The interactive scheme, incorporating the solution of the boundary-layer equations by the characteristic box scheme and with the numerical mesh determined in accordance with the stability criterion, has been used to calculate the laminar flow for a model problem. The numerical aspects of this procedure have been thoroughly tested and shown to be general so that it can be used for the solution of laminar and turbulent flows over airfoils of practical relevance.

7.0 REFERENCES

Carr, L.W., McAlister, K.W. and McCroskey, W.J., 1977, Analysis of the development of dynamic stall based on oscillating airfoil experiments, NASA TND-8382.

Cebeci, T., 1976, Separated flows and their representation by boundary-layer equations. Mech. Eng. Rept. ONR-CR215-234-2, California State University, Long Beach.

Cebeci, T., 1979, The laminar boundary layer on a circular cylinder started impulsively from rest, J. Comp. Phys. 31, 153-172.

Cebeci, T., 1982, Unsteady separation. In Numerical and Physical Aspects of Aerodynamic Flows (ed. T. Cebeci), Springer-Verlag, N.Y.

Cebeci, T., 1986, Unsteady boundary layers with an intelligent numerical scheme. J. Fluid Mech. 163, 129.

Cebeci, T. and Bradshaw, P., 1984, Physical and Computational Aspects of Convective Heat Transfer, Springer-Verlag, NY.

Cebeci, T. and Carr, L.W., 1981, Prediction of boundary-layer characteristics of an oscillating airfoil, In Unsteady Turbulent Shear Flows (R. Michel, J. Cousteix and R. Houdeville, eds.), Springer, 145-158.

Cebeci, T. and Clark, R. W., 1984, an interactive approach to subsonic flows with separation. In Numerical and Physical Aspects of Aerodynamic Flows, II (ed. T. Cebeci), Springer-Verlag, NY, 193-204.

Cebeci, T., Khattab, A.A. and Schimke, S.M., 1984, Can the singularity be removed in time-dependent flows? In Workshop of Unsteady Separated Flow (M.S. Francis and M.W. Luttges, eds.), Colorado Springs, CO.

Cebeci, T., Stewartson, K. and Williams, P.G., 1981, Separation and reattachment near the leading edge of a thin airfoil at incidence, AGARD CP 291, Paper 20.

Cebeci, T., Clark, R.W., Chang, K.C., Halsey, N.D. and Lee, K., 1986, Airfoils with separation and the resulting wakes, J. Fluid Mech. 163, 232.

Cowley, S.J., 1983, Computer extension and analytic continuation of Blasius' expansion for impulsive flow past a circular cylinder, J. Fluid Mech. 135, 389-405.

Daley, D.C. and Jumper, E.J., 1984, Experimental investigation of dynamic stall. J. of Aircraft 21, 831-832.

Francis, M.S., Keese, J.E. and Retelle, J.P., Jr., 1983, An investigation of airfoil dynamic stall with large amplitude motions, FJSRL-TR-83-0010, F.J. Seiler Research Labs, Air Force Academy, Colorado Springs, CO.

Ingham, D.B., 1984, Unsteady separation, J. Comp. Phys. 53, 90-99.

Isaacson, E. and Keller, H.B., 1966, Analysis of Numerical Methods, John Wiley, N.Y., 1966.

Keller, H.B., 1974, Accurate difference methods for two-point boundary-value problems, SIAM J. Num. Anal. 11, 305.

Keller, H.B., 1978, Numerical methods in boundary-layer theory, Ann. Rev. Fluid Mech. 10, 417-433.

Krause, E., Hirschel, E.H. and Bothemann, Th., 1968, Die numerische integration der bewegungsgleichungen dreidimensionaler laminarer kompressibler grenzschichten, Bond 3, Fachtagung Aerodynamik, Berlin; D6LR-Fachlinchreike.

Lorber, P.F. and Covert, E.E., 1986, Unsteady airfoil boundary layers - experiment and computation, in Numerical and Physical Aspects of Aerodynamic Flows III, (ed. T. Cebeci), Springer-Verlag, NY, 235-251.

Stewartson, K., Smith, F.T. and Kaups, K., 1982, Marginal separation. Studies in Applied Mathematics 67, pp. 45-61.

van Dommelen, L.L. and Shen, S.F., 1982, The genesis of separation, Numerical and Physical Aspects of Aerodynamic Flows (T. Cebeci, ed.), Springer-Verlag, N.Y., pp. 293-311.

Veldman, A.E.P., 1981, New quasi-simultaneous method to calculate interacting boundary layers, AIAA J. 19, 79-85.

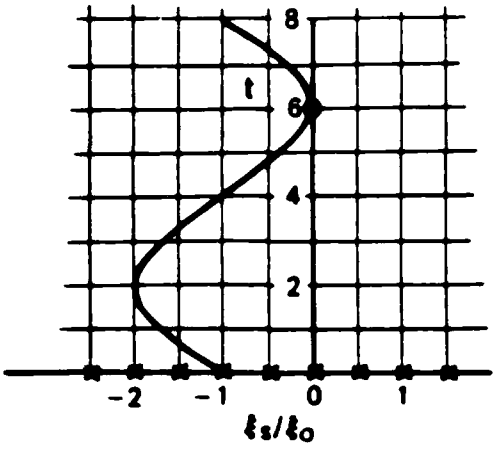

Figure 1. Variation of stagnation point with time for one cycle according to Eq. (10) with A = 1, $\omega = \pi/4$.

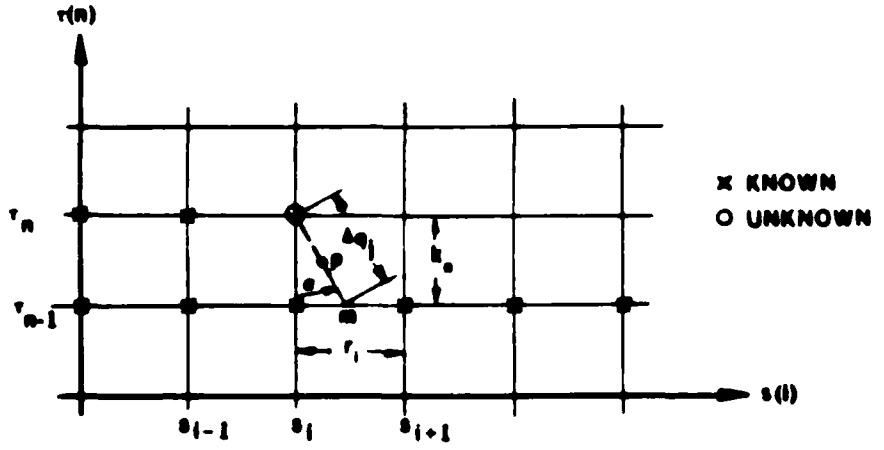

Figure 2. Notation for the characteristic box scheme.

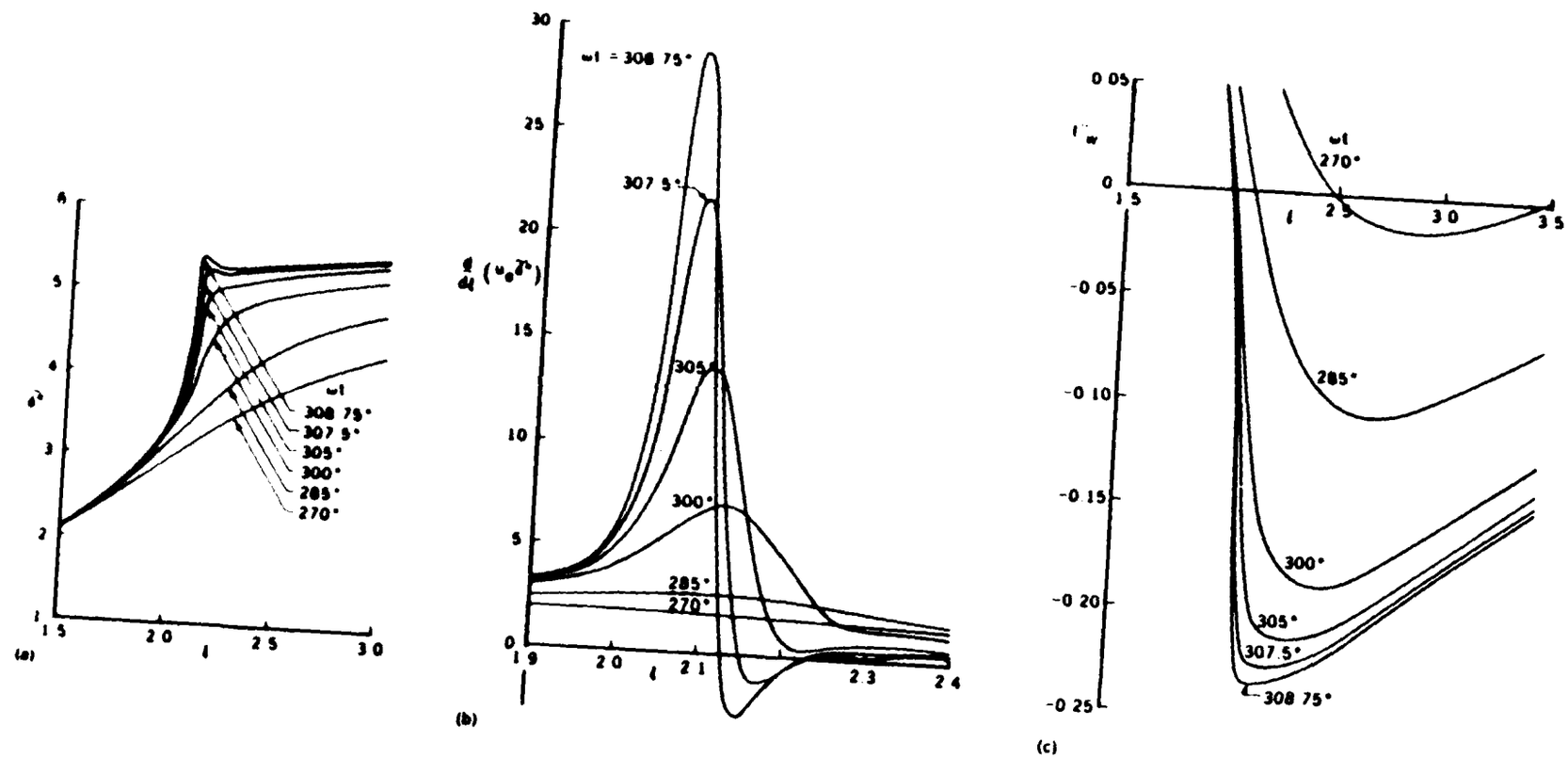

Figure 3. Variation of: (a) displacement thickness, $\tilde{\delta}^*$, (b) displacement velocity, $d/d\xi(u_e\tilde{\delta}^*)$, and (c) wall shear parameter, f''_w, with ξ for the oscillating airfoil, A = 1, ω = 0.1.

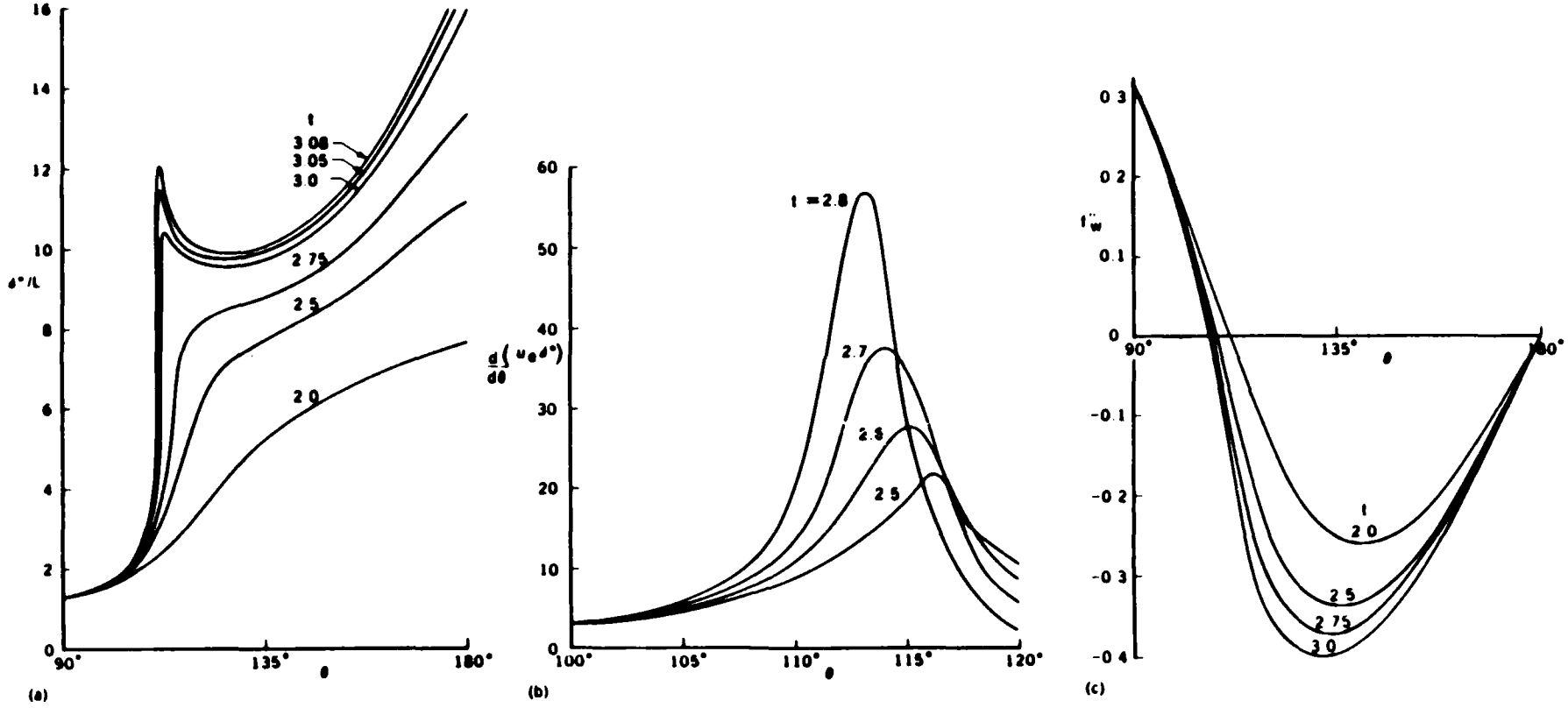

Figure 4. Variation of: (a) displacement thickness, δ^*, (b) displacement velocity, and (c) wall shear parameter with θ for the circular cylinder.

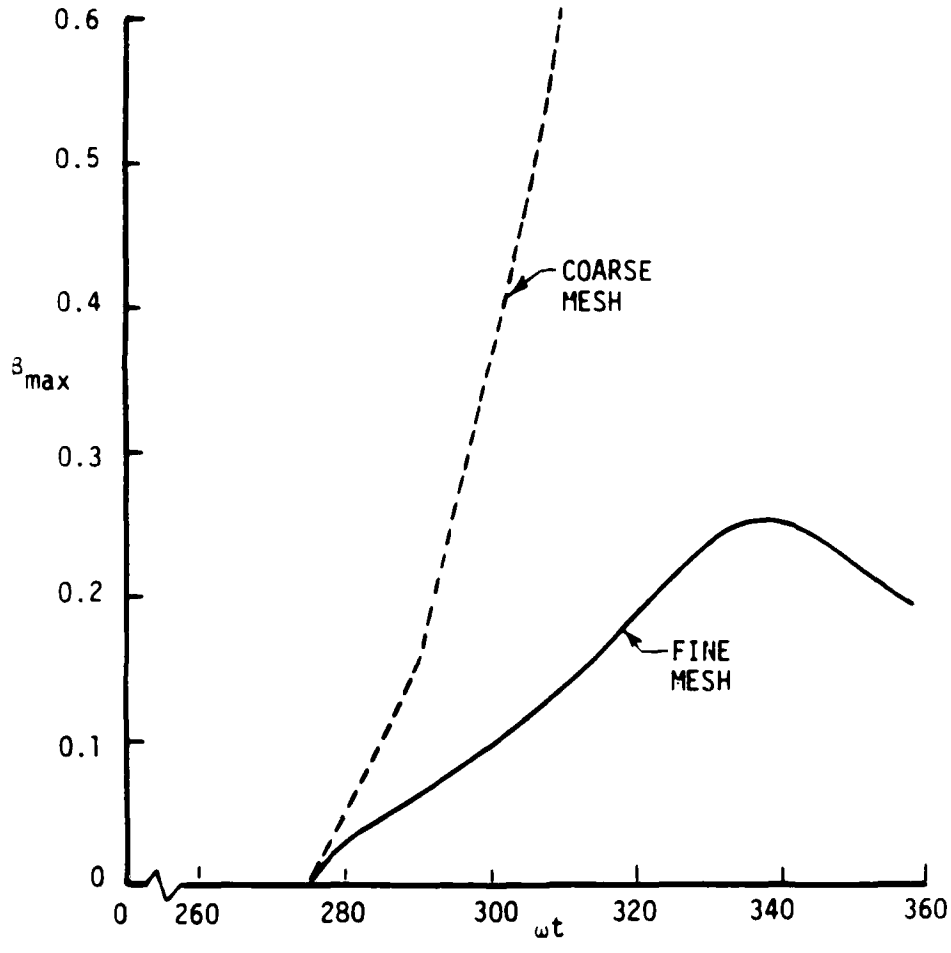

Figure 5. Effect of the coarse and fine meshes on the variation of the stability parameter β with ωt.

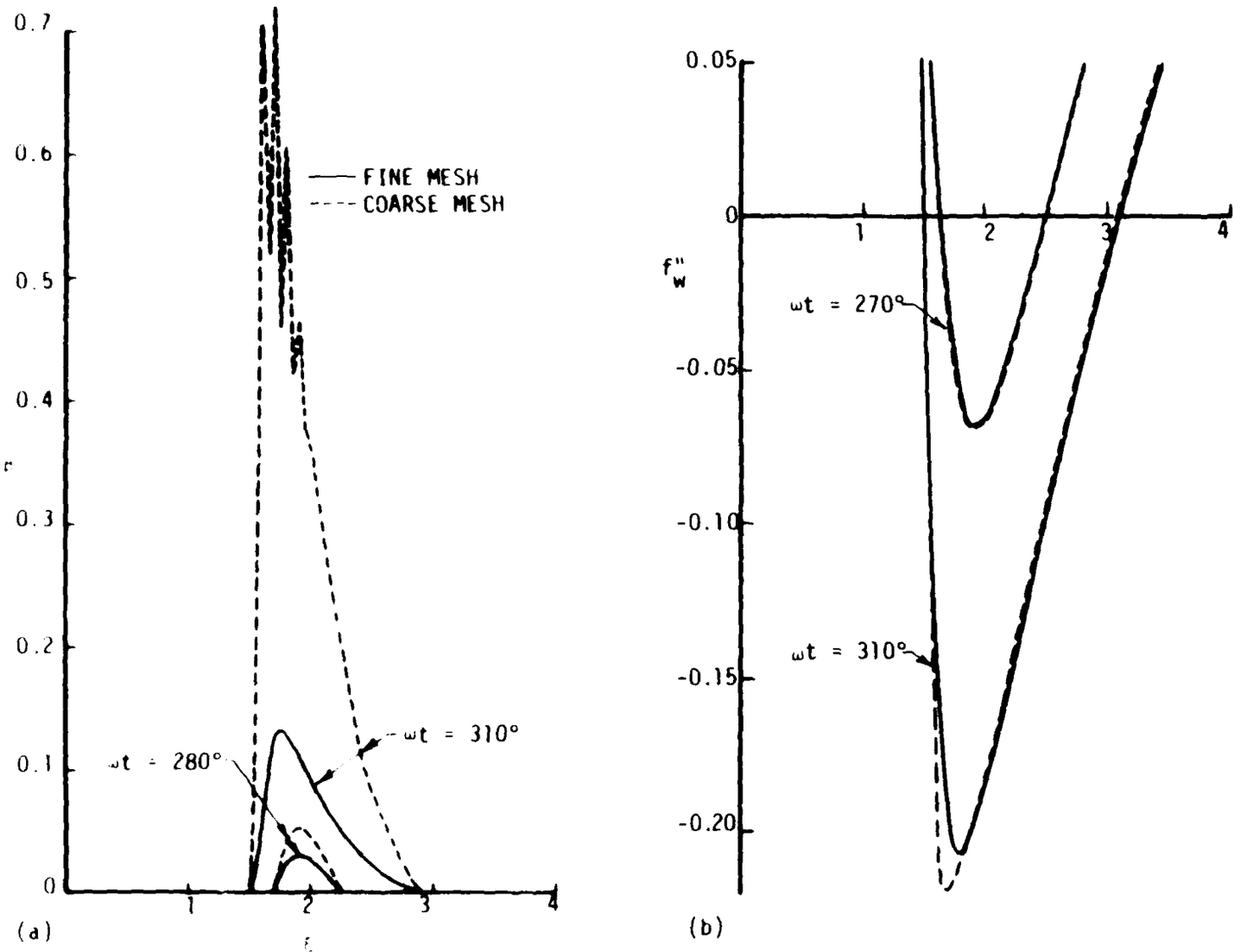

Figure 6. Effect of the coarse and fine meshes on the variation of the (a) stability parameter β, and (b) wall shear f''_w with ξ.

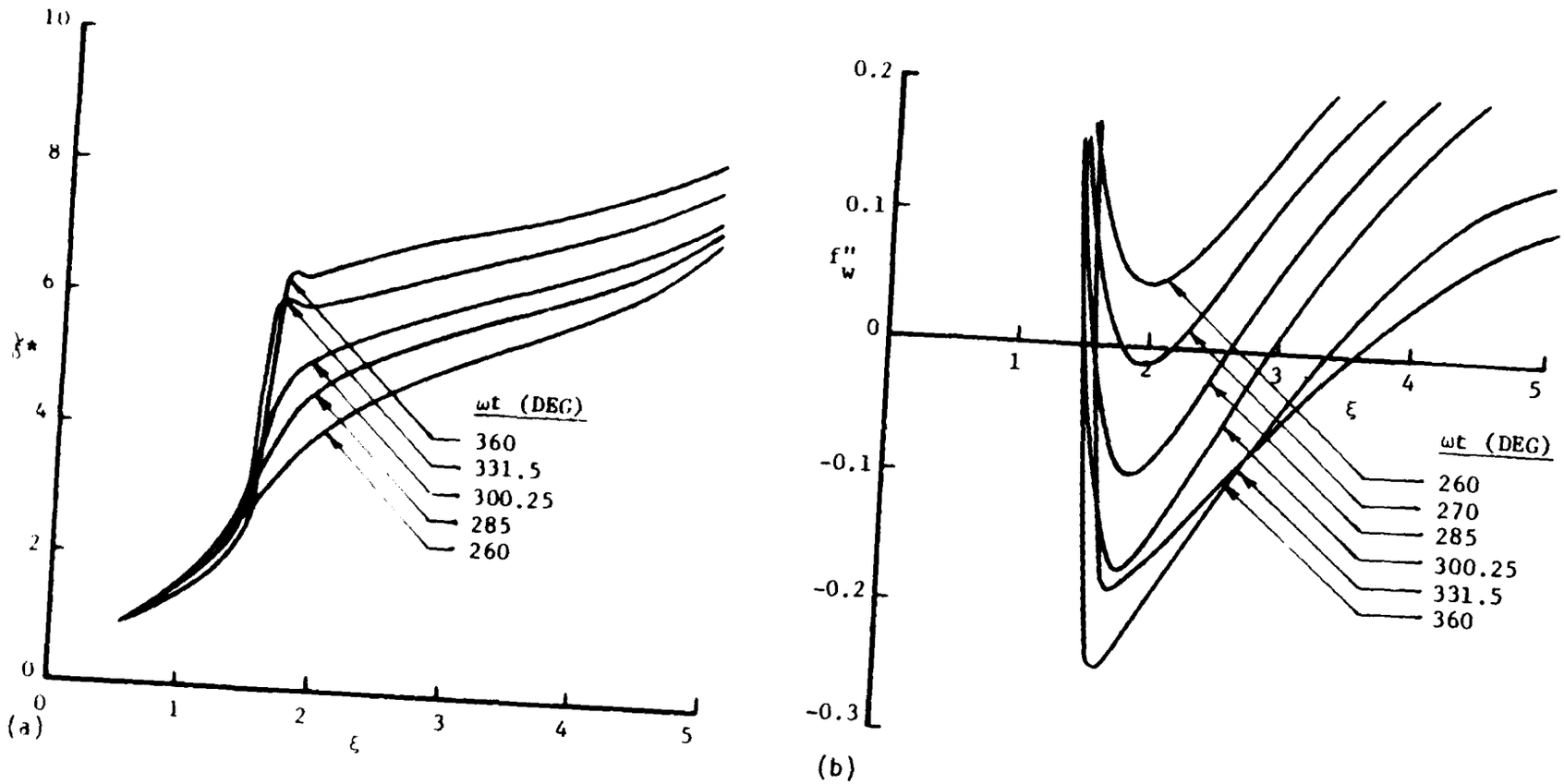

Figure 7. Results obtained with the characteristic box scheme for $\omega = 0.1$. Variation of (a) displacement thickness δ^* and (b) wall shear f''_w with ξ.

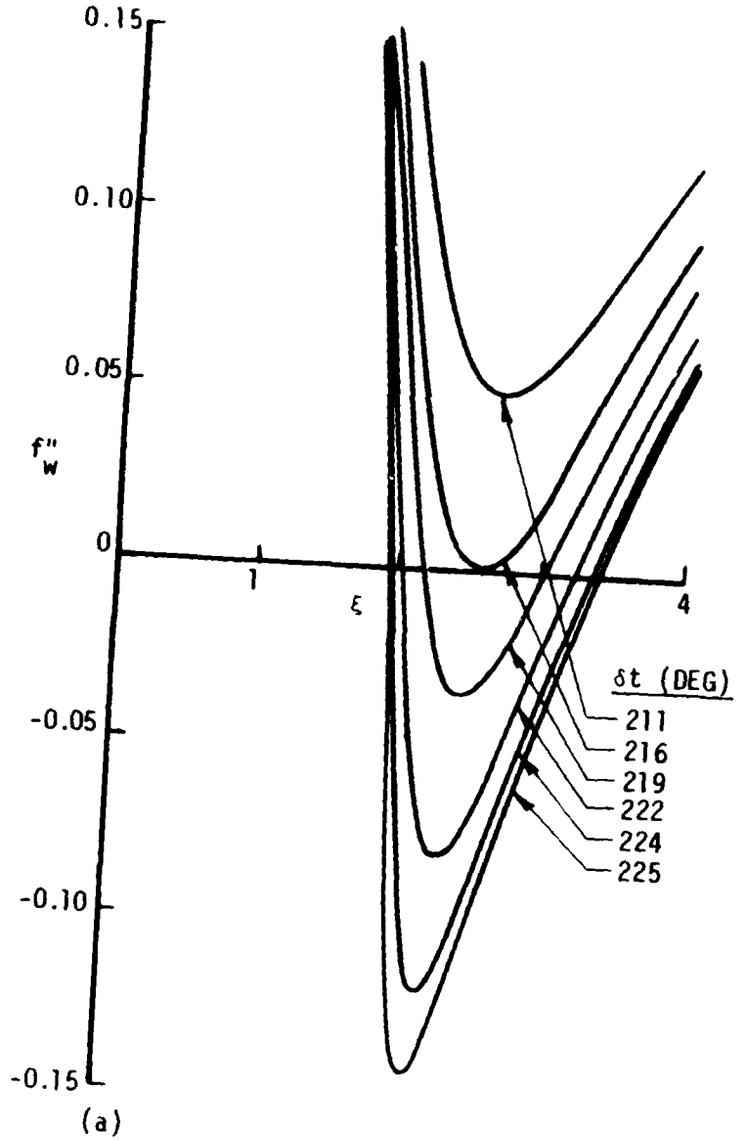

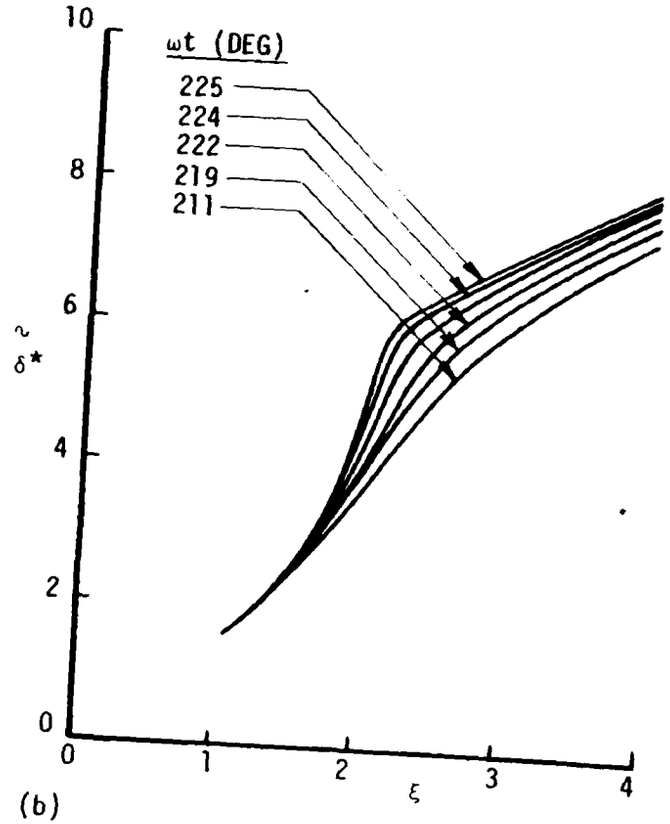

Figure 8. Variation of (a) wall shear f''_w and (b) displacement thickness $\tilde{\delta}^*$ with ξ for $\omega = 0.01$.

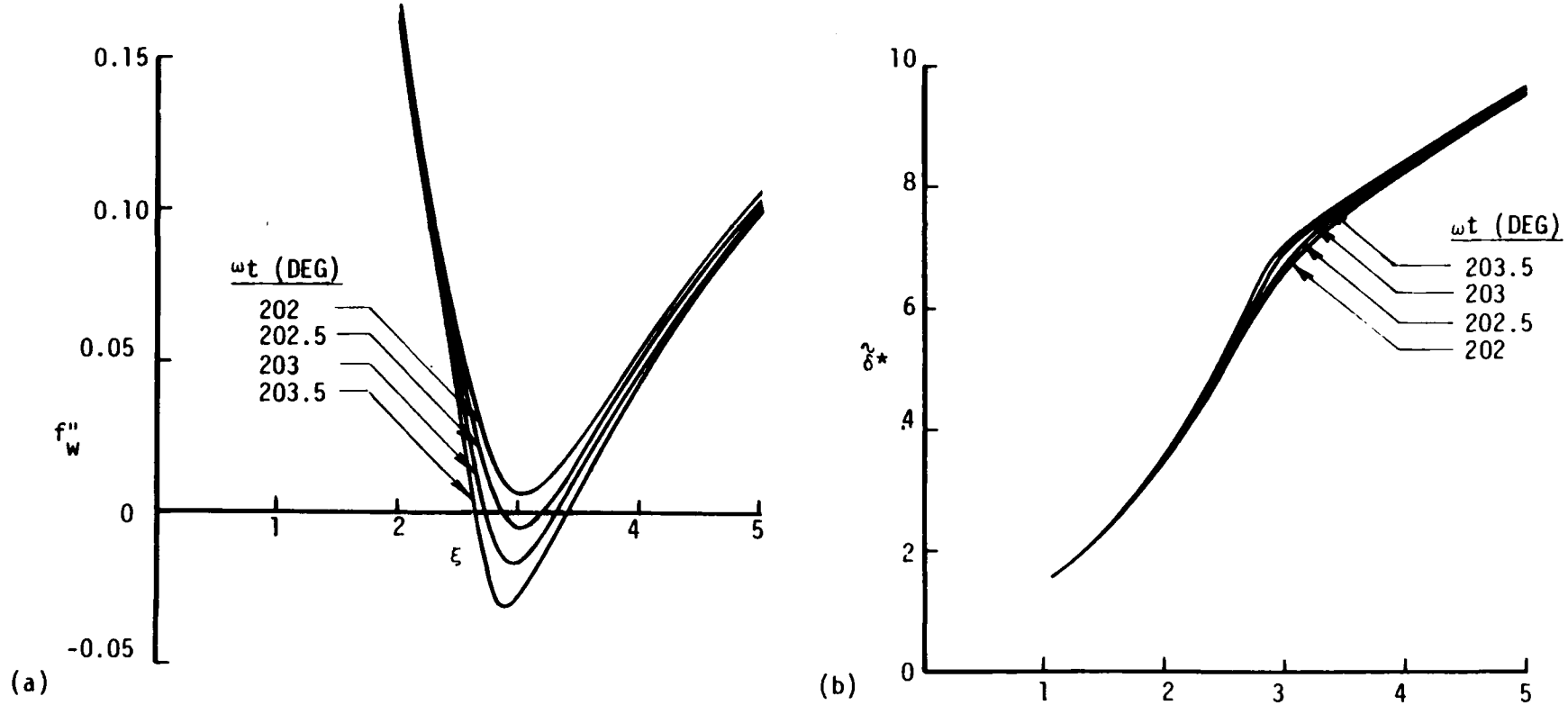

Figure 9. Variation of (a) wall shear f''_w and (b) displacement thickness $\tilde{\delta}^*$ with ξ for $\omega = 0.001$.

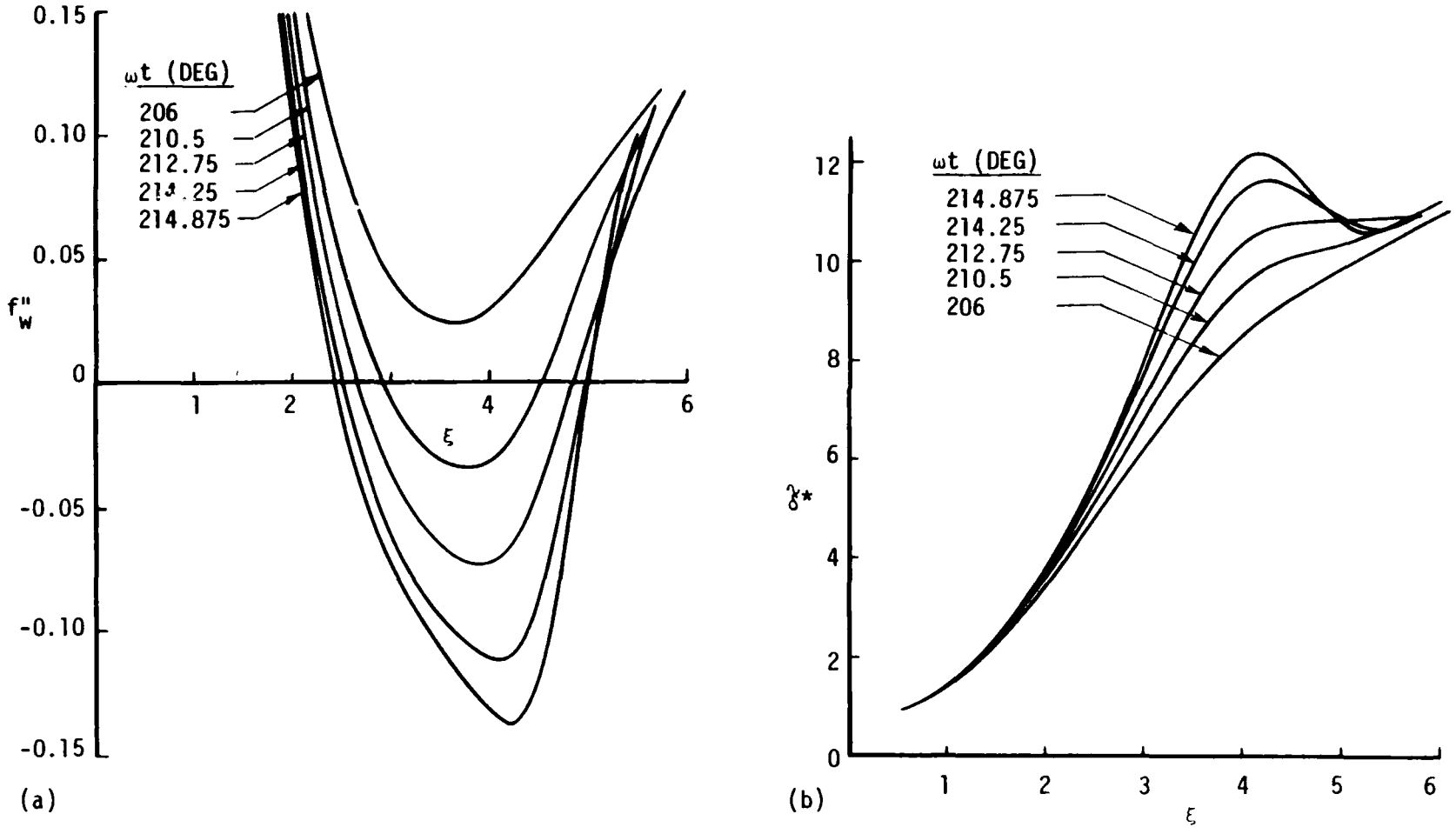

Figure 10. Effect of interaction on the variation of (a) wall shear f''_w and (b) displacement thickness γ^* for $\omega = 0.001$ and $\varepsilon = 10^4$.

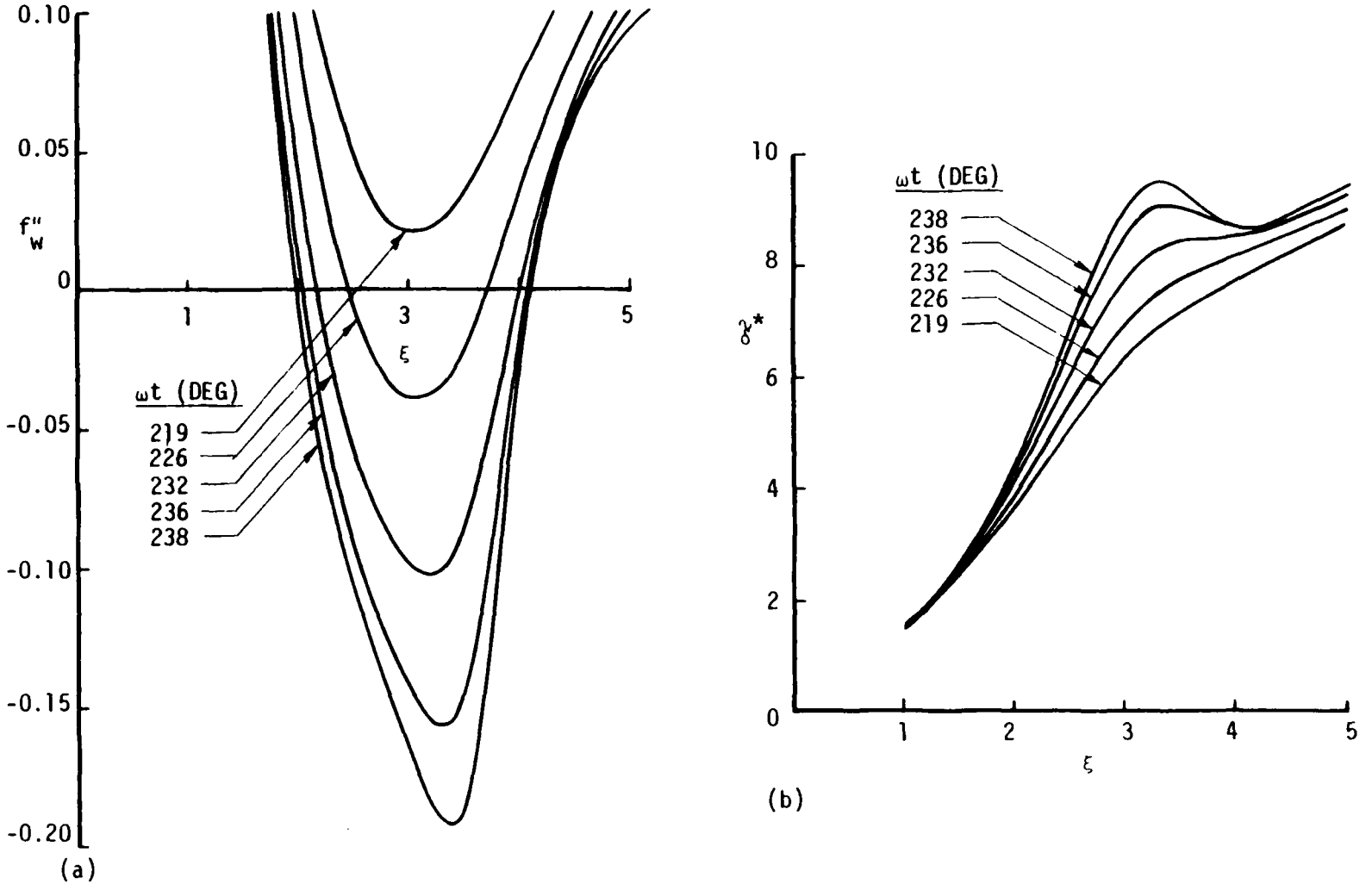

Figure 11. Effect of interaction on the variation of (a) wall shear f''_w and (b) displacement thickness δ^* with ξ for $\omega = 0.01$ and $\varepsilon = 10^4$.

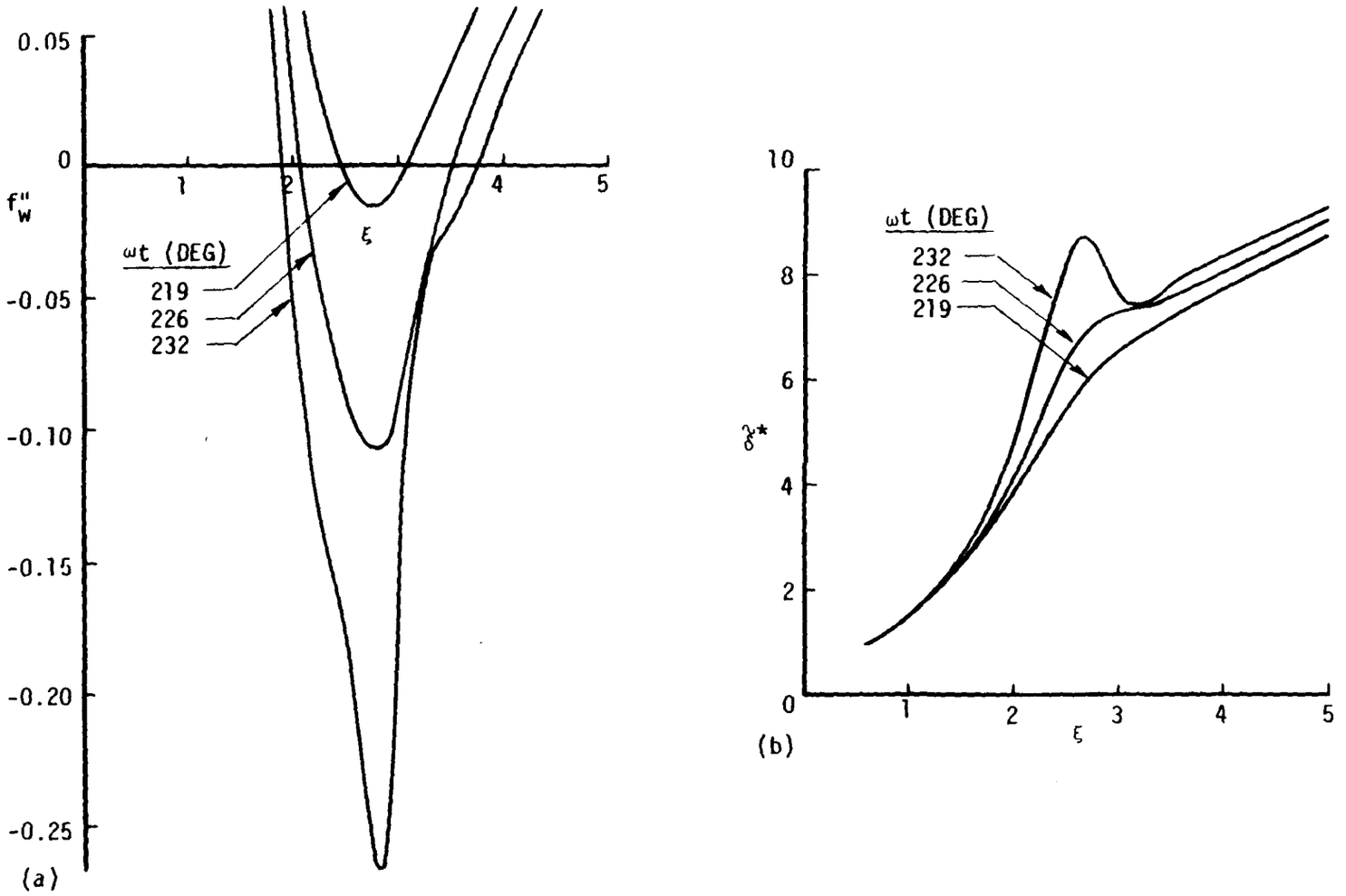

Figure 12. Effect of interaction on the variation of (a) wall shear f''_w and (b) displacement thickness $\tilde{\delta}^*$ with ξ for $\omega = 0.01$ and $\epsilon = 10^{-5}$.

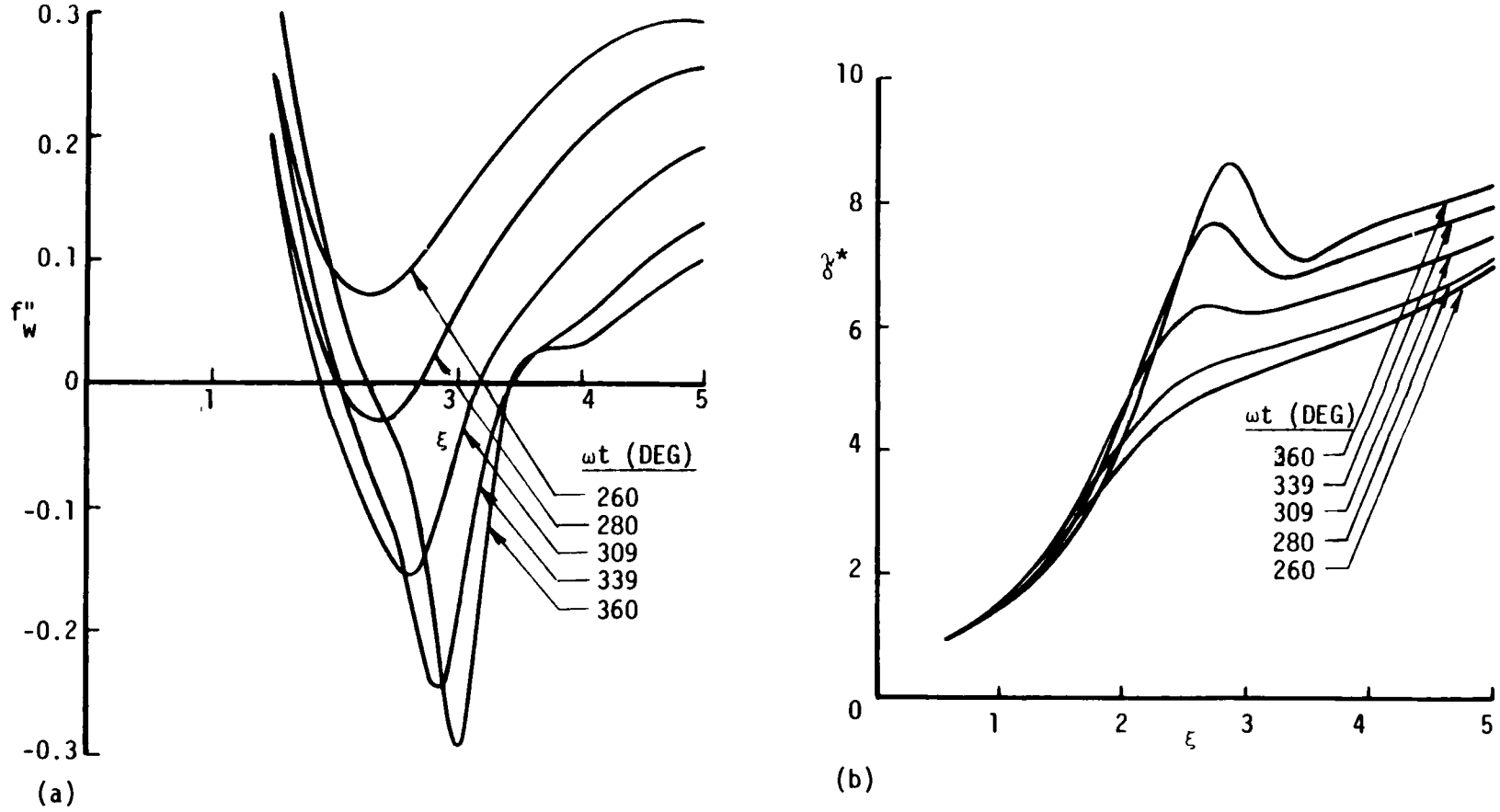

Figure 13. Effect of interaction on the variation of (a) wall shear f''_w and (b) displacement thickness $\tilde{\delta}^*$ with ξ for $\omega = 0.1$ and $\varepsilon = 10^4$.

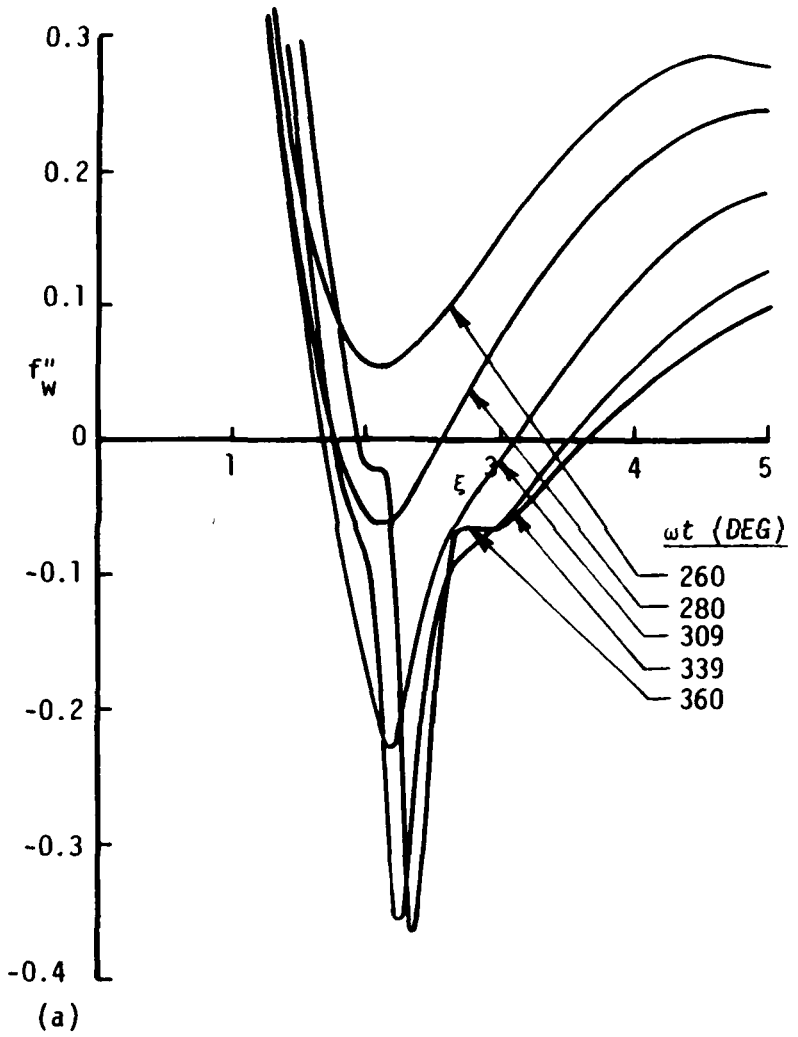

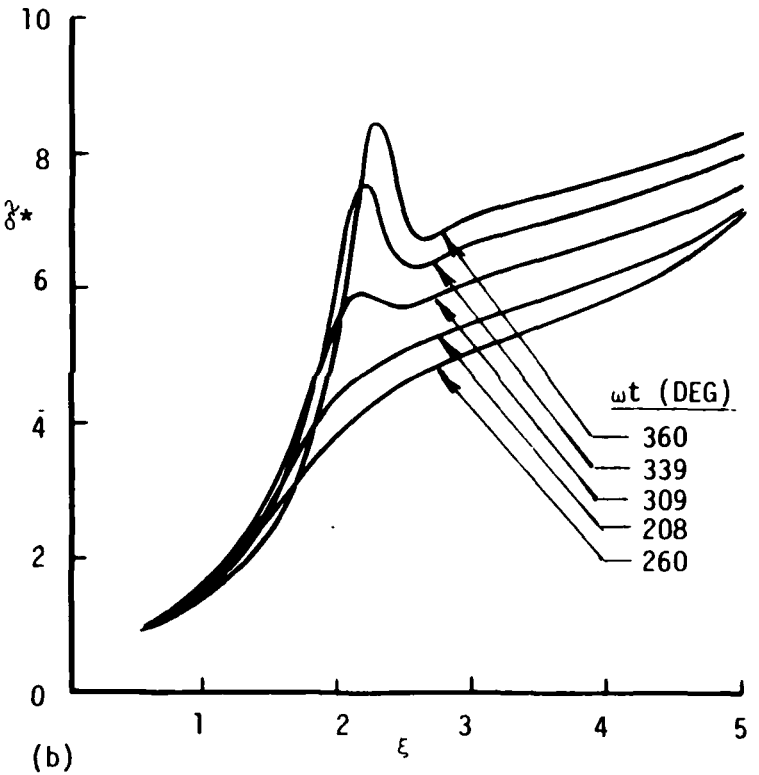

Figure 14. Effect of interaction on the variation of (a) wall shear f''_w and (b) displacement thickness δ^* with ξ for $\omega = -.1$ and $\varepsilon = 10^5$.

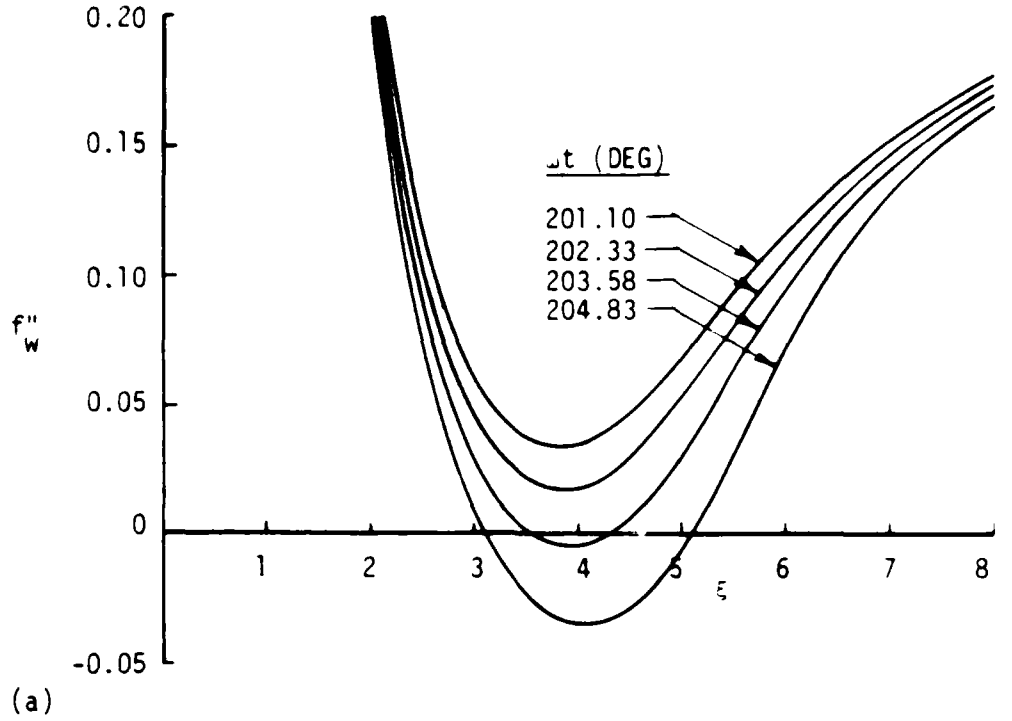

(a)

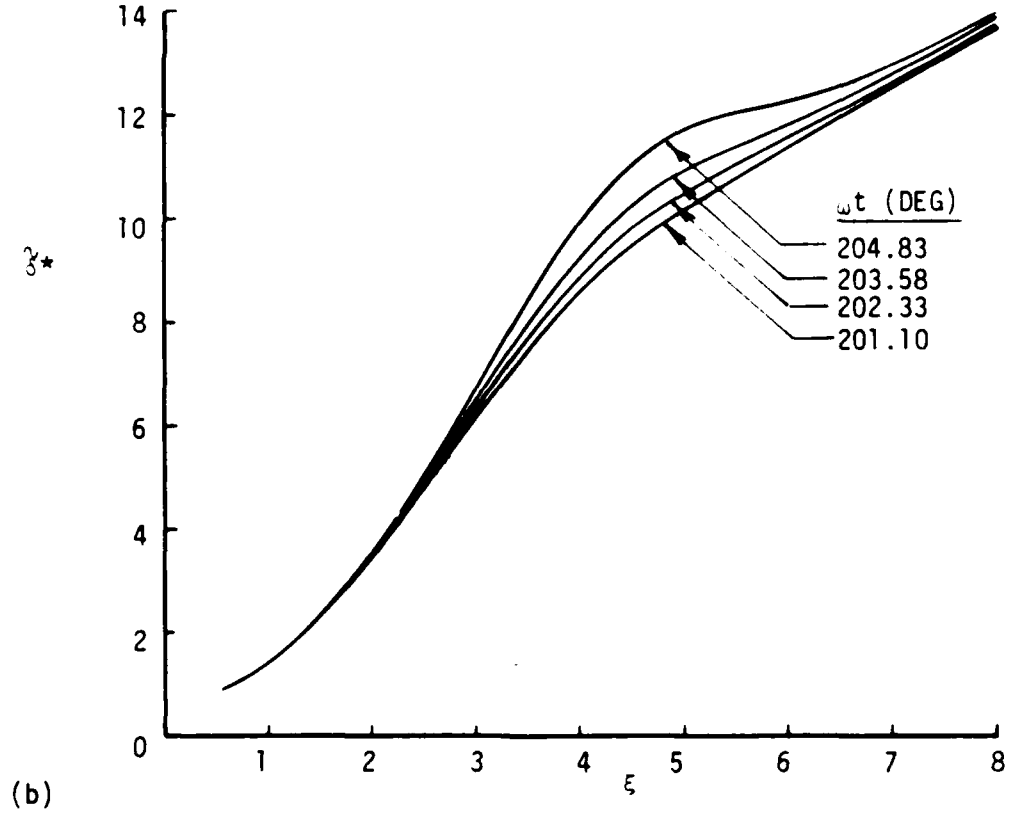

(b)

Figure 15. Effect of interaction on the variation of (a) wall shear f''_w and (b) displacement thickness δ^* for a steady flow at $\varepsilon = 10^4$.

END

8-87

DTIC